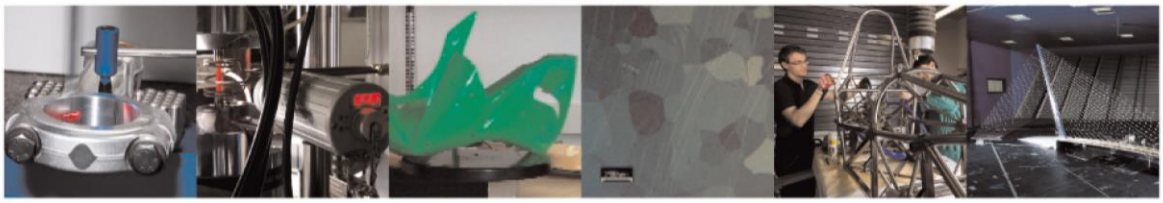

Estimation of melt pool size by complementary use of external illumination and process emission in coaxial monitoring of selective laser melting

Pacher, M., Mazzoleni, L., Caprio, L., Demir, A.G., Previtali, B.

DIPARTIMENTO DI MECCANICA ■ POLITECNICO DI MILANO
via G. La Masa, 1 ■ 20156 Milano ■ EMAIL (PEC): pecmecc@cert.polimi.it
http://www.mecc.polimi.it
Rev. 0

Estimation of melt pool size by complementary use of external illumination and process emission in coaxial monitoring of selective laser melting

Matteo Pacher[1], Luca Mazzoleni[1], Leonardo Caprio[1], Ali Gökhan Demir[1] and Barbara Previtali[1]

[1] Department of Mechanical Engineering, Politecnico di Milano, Via La Masa 1, 20156 Milan, Italy

Abstract

Coaxial imaging of melt pool dynamics provides several advantages over other monitoring methods in SLM. The ability to track the processing zone ensures the possibility to observe defect formation dynamics mainly related to melting and solidification. Commonly, the melt pool dynamics are observed by means of process emission. In process emission images, geometrical information of the melt pool are not directly available and their extraction would require the use of a calibrated sensor in order to measure the temperature levels; as a consequence commonly an arbitrary threshold is applied to the image. The use of external illumination for monitoring purposes allows for suppressing the process emission and observing the melt pool geometry by means of the reflected light. On the other hand, the obtained images show lower contrast and can be difficult to process by means of image processing algorithms. Accordingly, this work proposes the complementary use of external illumination and process emission for characterizing the melt pool dynamics in SLM. For the purpose, an open SLM platform with an inhouse designed coaxial monitoring module is used. Images with external illumination were used to estimate the melt pool size for AISI 316L. The information was used to set a threshold value for determining the melt pool size observed at the near infrared emission band. The proposed strategy proved promising for real time monitoring and control applications and can represent a feasible solution for industrial systems.

I. Introduction

Selective laser melting (SLM) has recently gained attention from the industrial scenario thanks to the flexibility and the ability of realizing complex shapes. Albeit the SLM technology results as established in some industrial fields such as aerospace, there are still several open issues that compromises the reproducibility of produced parts. To name a few, delamination, residual stresses, pores formation and cracking. The possibility to detect defect formation during the process is highly desired, in order to develop proper control actions for their prevention or correction.

This paper focuses on the use of both external illumination and process emission images to estimate the melt pool dimensions. As known, the use of external illumination with an adequate external lighting source offers the chance to observe the melt pool geometry. Then, its dimensions can be estimated with adequate algorithms. The main limitations of such approach rely on the high cost of proper lighting sources and on the design of the image analysis algorithm. As a result, this technique is usually adopted in the context of understanding the physical behaviour of the process and/or the mechanisms of formation of defects [1], [2]. On the other hand, process emission offers different information that are usually related with defects formation or particular process behaviours [3]. Different emission bands can be used to highlight different phenomena such as spatter emission or melt pool shape [4-5].

The proposed strategy combines external illumination and process emission for fast geometrical characterization of the melt pool. Melt pool length, width and area are estimated from process emission images after a calibration with externally illuminated ones is performed. The novelty of that approach is twofold:

- externally illuminated images are taken as reference as in [6-7] but *quantitative* estimation of geometrical features is performed;
- an optimization is run to make estimates coming from externally illuminated images and process emission ones match in average sense.

The final method combines the advantages of both sources of information: geometrical identification of the melt pool and fast computation thanks to the application of simple image analysis. The presented monitoring architecture is promising for achieving real time performances and, thanks to the limited cost of the equipment, this technique could be implemented also in

industrial systems to monitor and control melt pool shape.

II. System and materials

A. Selective laser melting platform

In this work, an open and custom-made SLM system was used [8-9]. The powder bed, placed in a sealed chamber, has a working area of 60x60mm^2 and can process small amount of powder (less than 0.5kg); An inertization procedure is performed three times before to processing; it consists in a cycle of vacuum till -950mbar followed by Ar pumping until a pressure of 10mbar is reached. The powder bed movement and the pressure control are implemented in LabVIEW environment (National Instruments, Austin, TX) where the machine status is monitored. Finally, the other process parameters, namely, scan path trajectory, laser power and scan speed are set using SCANMASTER software (Cambridge Technologies, Bedford, MA).

The laser source is a single mode fiber laser with 250W maximum power (IPG Photonics YLR-150/750-QCW-AC, Cambridge, MA, USA). The collimation lens out of the fiber has a focal length of 50mm and the focal position is regulated via a zoom optic (VarioScan 20, Scanlab GmbH, Puchheim, Germany) placed after the collimation lens. The beam is then manipulated by a scanner head (HurryScan 14, Scanlab GmbH, Puchheim, Germany) and focused by a 420mm f-theta lens. Finally, the waist diameter is calculated as 70µm.

Table 1: Main characteristics of the SLM prototype.

Working volume, *DxWxH*	60x60x20mm^3
Laser wavelength, λ	1070nm
Max. laser power, P_{max}	250W
Beam quality factor, M^2	1.1
Nominal waist diameter, d_0	70µm
Vacuum capabilities	-950mbar

B. Monitoring module

The monitoring module is mounted coaxially and is inserted between the scanner head and the zoom optic. The image plane is fixed and regulated thanks to a professional camera lens system (Camera Adapter, Scanlab GmbH, Puchheim, Germany) having and equivalent focal length of 120mm; the camera lens system includes also a dichroic mirror transparent to the laser radiation and reflective between 400-1000nm. The image plane is set equal to the processing plane and the collected light passes through the f-theta lens, the scanner head (galvanometric mirrors), the dichroic mirror and the camera lens before reaching the sensor. Furthermore, optical filters are inserted between the camera and the camera lens to capture different process emission bands or the band of the external lighting source.

The chosen camera sensor is an industrial CMOS camera (Ximea xiQ USB Vision, Münster, Germany) based on Si photodetectors with a sensitivity between $350 - 1000$nm. Sensor size and pixel size are respectively 1280x1024px^2 and 4.8x4.8µm^2; the camera permits to adjust the region of interest that influences both spatial and temporal resolution. Optical magnification and pixel number are designed to observe a field of view of 4.3x4.3mm^2 with $r_s = 14$µm/pixel as spatial resolution; according to the sensor capabilities the frame rate is set to 1200fps. Spatial resolution was measured using a calibrated metric stage micrometer used in common practice to calibrate microscopes (Leica 10310345, Wetzlar, Germany).

An external lighting source emitting at 640nm (Cavitar, Cavilux HF, Tampere, Finland) is used to observe the melt pool geometry. The lighting source is a low-coherent source with maximum power of 280W which is mounted laterally to the chamber and collimated on the working area. Light emission and camera frame acquisition are synchronized. To avoid back reflection of the processing laser into the monitoring module, a short pass filter at 1000nm is inserted before the sensor (Thorlabs, FESH1000, Newton, NJ, USA). In addition, two different optical filters are used to observe melt pool geometry and process emission respectively:

- a band pass filter at 650 ± 40nm is used to filter the reflected external light (Thorlabs, FB650-40, Newton, NJ, USA);
- a long pass filter at 850nm (Thorlabs, FEL0850, Newton, NJ, USA) is implemented to observe NIR process emission [4] in the range $850-1000$nm and is used without external light emission.

Fig. 1 depicts the system configuration.

Data analysis is done on a DELL XPS 15" with an Intel i7 processor (7-th generation). The code was implemented in MATLAB programming language and compiled thanks to the MATLAB compiler tool.

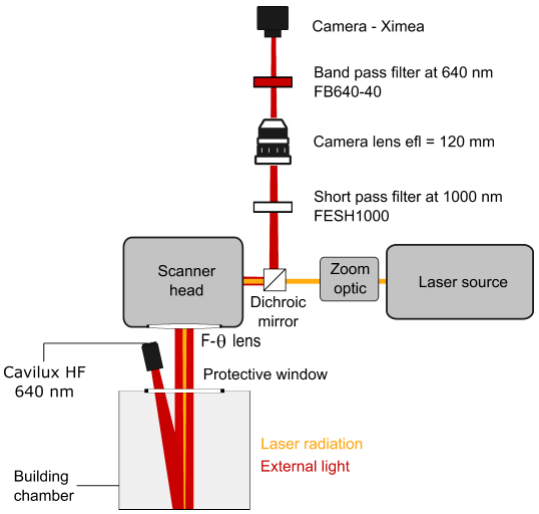

Figure 1: Schematic of the SLM system with the monitoring module employed in this work.

C. Materials

Powder in use is gas atomized AISI 316L stainless steel (Cogne Acciai, Brescia, Italy). The powder size distribution is D10:19.7µm, D50:29.8µm, D90: 44.6µm. Finally, the apparent density is 4.07g/cm3.

III. Experiments

A simple test geometry is produced as depicted in Fig. 2. The scan direction is always vertical, i.e. parallel to the shorter side of the thin walls. Laser power is set to 200W and scan speed to 400mm/s.

Hatch distance and layer thickness were 70µm and 50µm respectively. As aforementioned, the laser focal position is on the powder bed surface. These parameters were determined from preliminary experiments and proved to produce fully dense components. Process parameters are summarized in Table 2.

Table 2: Process parameters.

Laser power	200W
Scan speed	400mm/s
Hatch distance	70µm
Layer thickness	50µm

Video of the process have been acquired switching from externally illumination to process emission and vice versa layer by layer. Monitoring parameters namely frame exposure, optical filtering, power of the external

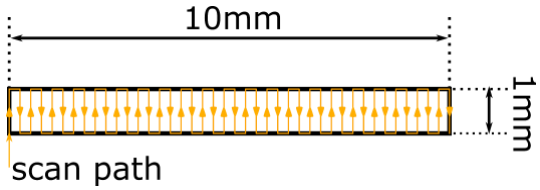

Figure 2: Schematic of the scanned geometry.

light source and pulse duration were adjusted during the preliminary tests as well.

Even if the video acquisition was not simultaneous, results of the following sections are considered valid; indeed considerations on melt pool measurements are done in average sense. Videos that have been compared together have been acquired in similar conditions, where the process is considered stable. Moreover, only layers after the 10th one have been considered during the analysis where the melt pool size stabilizes. In the first layers, the effect of the build substrate on heat flow conditions is relevant [10]. In fact, it features a high thermal conductivity, up to two orders of magnitude higher than powder material [11]. Conductive dissipation of thermal energy through the platform leads to a reduced melt pool area, since the energy input is brought away from the layer material interaction zone.

IV. Data Analysis Algorithms

In this study a method for fast data analysis is developed. Externally illuminated images are used at first as reference to calibrate estimates extracted from process emission images. Geometrical estimates are eventually extracted from process emission images achieving potentially real time performances.

Fig. 3 shows the workflow of the proposed method. Estimates of the area, length and width of the melt pool are initially collected from externally illuminated images using the DBSCAN (Density Based Spatial Clustering of Applications with Noise) algorithm [12]. These estimates are used to set the threshold for the Hard Thresholding Based (HTB) algorithm via optimization. Finally, temporal behaviours of area, length and width of the melt pool are extracted from process emission images in a faster and low-demanding way.

A. Analysis of externally illuminated images – DBSCAN

Fig. 4a shows an example of images acquired with external illumination. Albeit the melt pool is clearly visible as a dark blob, its extraction is not trivial: low image contrast makes simple algorithms based on gradient analysis and thresholding fail. The melt pool is recognized by human eye because it is a *localized* area

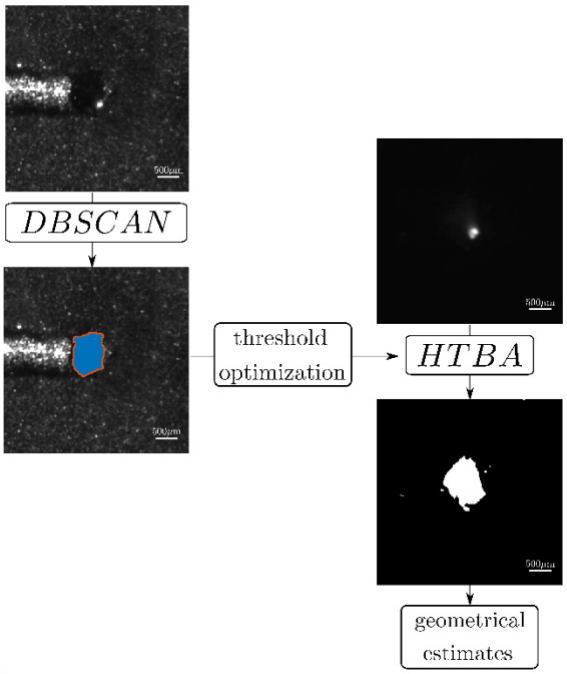

Figure 3: Example of image acquired with external illumination. The melt pool appears as a dark blob.

of the image with similar characteristics. In this framework, feature extraction should take into account spatial information. Given this type of database, a clustering algorithm was chosen because it classifies different regions of the image based on proper statistics.

The DBSCAN algorithm is the reference algorithm for what concerns density-based clustering [13]; some of its advantages are good clustering performances, limited computing time, recognition of arbitrary shape clusters and no requirements of data models [13-14]. The main idea of density-based algorithms is that a cluster is dense of points with similar characteristics. Similar characteristics are described thanks to a distance function that considers the features of interest (e.g. the gray level and closeness of points). In addition, dense means that there is a minimum number of close points in a localized area. The algorithm needs two parameters: the minimum number of elements, *minPnts,* and the maximum distance between two different points, ε. The complete description of the DBSCAN algorithm can be found in [12]. For sake of briefness details are not provided here while the proposed implementation and the calculation of the geometrical parameters of the melt pool are described.

An image is a matrix $I \in \mathbb{R}^{m\times n}$, with $m, n \in \mathbb{N}$ being the number of rows and columns respectively. Each element of the matrix is a pixel with gray level value $g_{i,j} \in [0,255]$. Each pixel can be represented as a vector $p_k \in N^3, \mathrm{k} \in [1, m \cdot n]$ defined as

$$\mathrm{p_k} = \begin{pmatrix} \mathrm{i} \\ \mathrm{j} \\ \mathrm{g_{i,j}} \end{pmatrix}, \tag{1}$$

where $\mathrm{i} \in [1, \mathrm{m}]$, $\mathrm{j} \in [1, \mathrm{n}]$ are the rows and columns indexes of matrix I identifying the pixel and $g_{i,j}$ is its gray level (also called intensity in the following paragraphs). We are therefore considering a dataset composed by points p_k that represents the two spatial coordinates of a pixel and its intensity value. The distance function is accordingly defined as the Euclidean distance between two points

$$\mathrm{d(h,k)} = \|p_h - p_k\|_2 . \tag{2}$$

The algorithm then proceeds with two fundamental steps: neighbor identification and cluster expansion. Starting from an arbitrary point p_k, its neighbors $n_q \in \mathcal{N}_k$ ($\mathcal{N}_k$ being the set of neighbors of p_k) are all the points of the database satisfying

$$\mathrm{d(k,q)} < \varepsilon \quad \forall \mathrm{q} \in [1, \mathrm{m} \cdot \mathrm{n}], \mathrm{q} \neq \mathrm{k}. \tag{3}$$

If the number of neighbors is higher than *minPnts* then p_k is called *core point* and a new cluster is initialized. Otherwise, p_k is clustered as *noise*. If p_k is a core point, then the cluster is expanded to include all points that are close to each other.

The algorithm is run two times on two selected subsets of the image for the extraction of the melt pool and the laser irradiated zone respectively. Once clusters are identified some simple rules on cluster area and centroid positions have been implemented to identify the melt pool and the laser irradiated zone. Finally, the two clusters are joined, and the resulting region is filled. An example of the algorithm's output is showed in Fig. 4b. Constants *minPnts* and ε have been set equal to 150 and 9.75 respectively.

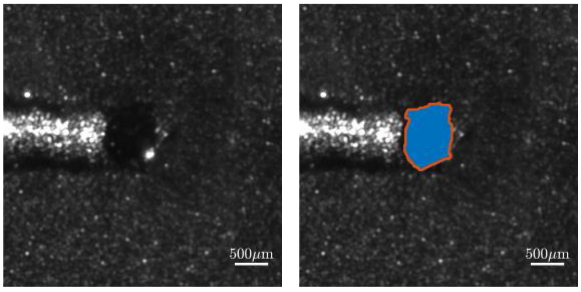

(a) (b)

Figure 4: Example of application of the image analysis algorithm based on DBSCAN for feature extraction.

Melt pool length is defined as the maximum dimension of the melt pool parallel to the scan direction. In the application under analysis, the scanning direction is always vertical, so the melt pool length is calculated as the difference between the maximum and the minimum vertical coordinate of the points in the melt pool multiplied by the scaling factor r_s (image resolution)

$$\hat{l} = r_s \left(\max_{k \in \mathcal{M}} p_k\,(2) - \min_{k \in \mathcal{M}} p_k\,(2) \right) \quad (4)$$

.

where $\mathcal{M}$ is the set of points that forms the melt pool. The melt pool width is defined as the maximum dimension of the melt pool perpendicular to the scan direction and is calculated as the melt pool length but considering the horizontal direction

$$\hat{w} = r_s \left(\max_{k \in \mathcal{M}} p_k\,(1) - \min_{k \in \mathcal{M}} p_k\,(1) \right). \quad (5)$$

The area is finally calculated as the cardinality of set $\mathcal{M}$ multiplied by the scaling factor squared

$$\hat{A} = r_s^2 |\mathcal{M}|. \quad (6)$$

B. Analysis of thermal emission images - HTB

Fig. 5a shows an example of process emission image. The gray level of images is related to temperature and can be used to identify the boundaries of the melt pool. As for the melt pool, it is observed also the emission coming from the spatters i.e. small particles of molten material ejected from the melt pool. In what follows, the algorithm for extracting the melt pool shape and isolating it with respect to spatters is explained.

Feature extraction is much easier in these conditions because of the simplicity of images. Gradient methods are not suitable because high gradient values are localized nearby the laser irradiated zone and not at the melt pool boundaries. Conversely, hard thresholding highlights the melt pool and spatters. Hard thresholding is defined as

$$\tilde{g}_{i,j} = \begin{cases} 1 & g_{i,j} \geq C \\ 0 & otherwise \end{cases}, \quad (7)$$

where $g_{i,j}$ is the gray level of the operand image I, $\tilde{g}_{i,j}$ is pixel value of the binary image, $\tilde{I}$, resulting from the operation and C is the value of the threshold. Once hard thresholding is applied to process emission images, the melt pool appears as a white blob together with spatters. Consequently, an analysis of regions is applied to the binary image $\tilde{I}$ to identify the melt pool and other spatters.

The region analysis allows us to compute the estimates of area, length and width of the melt pool removing the disturbances that affect other monitoring techniques (i.e. photodiodes), exploiting the advantage of having spatial information. Initially, all the connected regions of the binary image are identified and classified [15]; in other words, all the connected white blobs of the binary image are isolated from the whole image and enumerated. Afterwards, the melt pool is identified among all regions as the region characterized by the maximum area and the minimum blob centroid - image center distance (coaxial setup).

Once the melt pool is identified, the binary image $\tilde{I}$ is cleaned from the other spots and geometrical quantities are finally computed. The length of the melt pool is calculated as the maximum pixel sum evaluated on the columns of image $\tilde{I}$

$$\hat{l}_C = r_s \sum_{j=1}^{n} \tilde{g}_{i,j}. \quad (8)$$

In a similar fashion, the width of the melt pool is calculated as the maximum pixel sum evaluated on the image rows

$$\hat{w}_C = r_s \sum_{i=1}^{m} \tilde{g}_{i,j}. \quad (9)$$

Finally, the melt pool area is calculated as the total pixel sum of the image

$$\hat{A}_C = r_s^2 \sum_{i=1}^{m} \sum_{j=1}^{n} \tilde{g}_{i,j}. \quad (10)$$

Results of the proposed algorithm are shown in Fig. 5b.

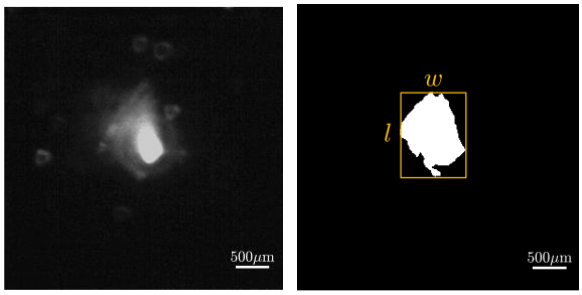

(a) (b)

Figure 5: Example of feature extraction of process emission images based on hard thresholding.

C. Calibration of process emission estimates

The threshold C in (7) for the calculation of geometrical quantities in (8)-(10) sensibly influences results: the bigger the threshold, the smaller the melt pool and vice versa. Accordingly, the estimates of area, length and width of the melt pool are function of C. Setting the threshold is therefore related to the selection of isotherm of the temperature that allows the distinction of the melt pool from the surrounding powder. As side effect, also spatters are identified because of their high temperature. This is not a big issue, since as aforementioned by a region analysis they can be easily filtered out.

Estimates of the melt pool computed by the DBSCAN algorithm are considered as reference; the target of the optimization is to make the estimates from externally illuminated images and the estimates from process emission images match in average sense. More specifically the following objective functions have been minimized

$$\begin{aligned} \mathrm{C_A} &= \min_{\mathrm{C}} (\overline{\mathrm{A}} - \overline{\mathrm{A}}_{\mathrm{C}})^2 , \\ \mathrm{C_l} &= \min_{\mathrm{C}} \left(\overline{\mathrm{l}} - \overline{\mathrm{l}}_{\mathrm{C}}\right)^2 , \\ \mathrm{C_w} &= \min_{\mathrm{C}} (\overline{\mathrm{w}} - \overline{\mathrm{w}}_{\mathrm{C}})^2 . \end{aligned} \tag{11}$$

where $\overline{(\cdot)}$ indicates the average of estimates. The three minimizations provide optimal threshold values for area, length and width respectively. It is observed that this optimization is convex and unconstrained. Since the optimization is convex and has converged, we can assure that the minimum is a global minimum and that it yields the optimum result in minimizing the objective function.

V. Results

A. Threshold calibration

Threshold calibration is performed analyzing images of a part of the entire geometry going from 1.5mm and 2.5mm of the total wall length corresponding to 30 frames. Results of the optimization (11) are shown in Fig. 6, where estimates computed with their optimized threshold are compared with reference values. As expected the minimization makes the two series of values match in average sense.

The threshold values are $C_A = C_l = 12$ and $C_w = 14$ and the difference of melt pool shape is shown in Fig. 7. The fact that the three threshold values do not converge to the same value means that there is a difference in shape between melt pool observed in externally illuminated images and process emission ones. Indeed, there is an agreement between area and length but not

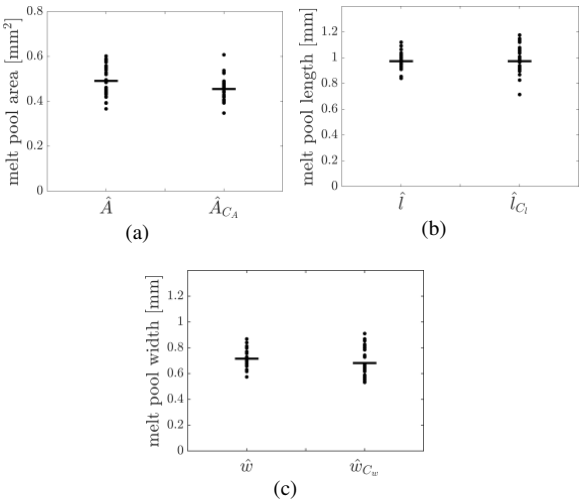

Figure 6: Results of the calibration procedure: the matching between reference and calibrated values is shown.

with melt pool width which is overestimated when keeping the threshold $C_A = C_l$. This could be motivated as follows:

1. estimates from DBSCAN algorithm provides a width which is slightly underestimated;
2. process emission at the melt pool tail (i.e. at the left) has a slow decay [7]. Estimates from process emission images tends to be

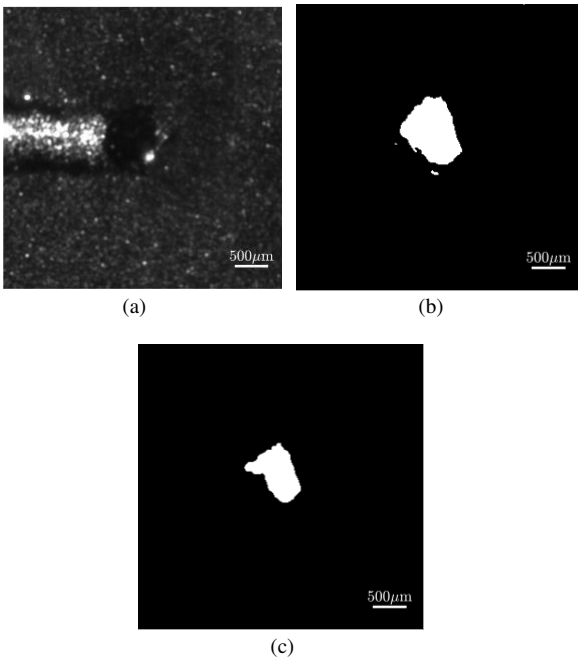

Figure 7: Differences in melt pool shape for different values of thresholds (b-c) compared with real melt pool (a). (b) and (c) shows the melt pool shape when $C_A = C_l$ or C_w respectively are chosen.

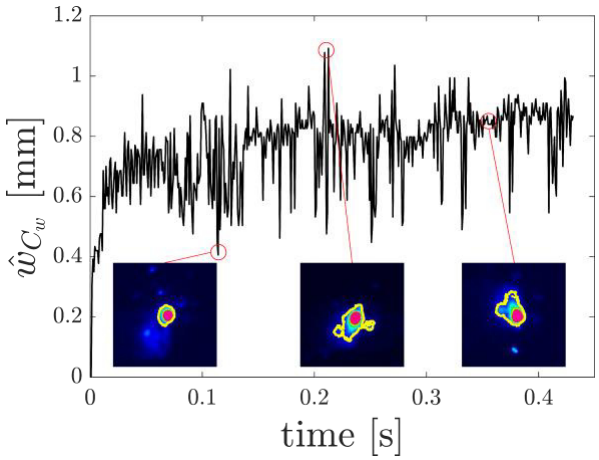

Figure 8: Melt pool width as a function of time (27th layer). The yellow contours in images correspond to melt pool shape identified by the HTB algorithm.

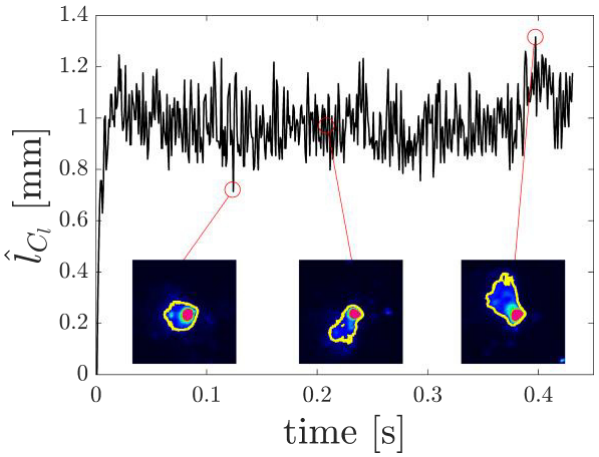

Figure 9: Melt pool length as a function of time (27th layer). The yellow contours in images correspond to melt pool shape identified by the HTB algorithm.

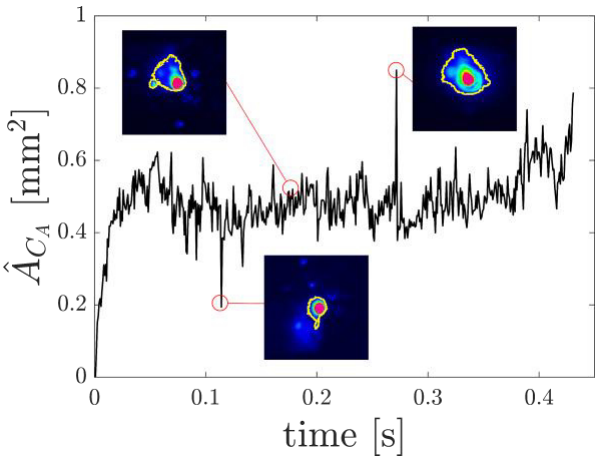

Figure 10: Melt pool area as a function of time (27th layer). The yellow contours in images correspond to melt pool shape identified by the HTB algorithm.

overestimated because of the emission of already solidified material.

Following studies will focus on a deep investigation about differences in melt pool shape given by process emission images and externally illuminated ones acquired simultaneously.

B. Melt pool dynamics

Fig. 8-10 show temporal behaviors of the melt pool estimates during the entire 27th layer. In Fig.8, local minima are related to positions where the laser spot changes direction (also called switching points in what follows): the algorithm recognizes only the laser irradiated zone because of the region analysis and lower melt pool emission due to the high laser spot – melt pool centroid distance. Furthermore, local maxima are related to spatters emission originated in the horizontal direction.

Considering Fig. 9, switching points are related by local maxima, whereas local minima are related to points where the laser irradiated zone is in central position. Furthermore, it observed that the behaviour of melt pool length is less nervous with respect to melt pool width. This is related to the high sensitivity of the HTB algorithm with respect to switching points when C_w is used. To overcome this issue, additional elements (e.g. neutral density filters) can be inserted in the optical chain to damp process emission in the laser irradiated zone [7]; this would result in higher values of threshold values and lower sensitivity of the HTB algorithm to its variation. It is hypothized that estimation performances would increase especially for width estimation.

The behaviour of melt pool area is depicted in Fig. 10; the same issue of sensitivity is observed but it happens only once. An increasing trend towards the end of the scanned geometry is observed. The effect of that trend on final quality has not been studied but can potentially lead to different processing conditions. The maximum value in the graph is related to a significantly bigger melt pool dimension again indicating some change in the processing conditions or the formation of a defect in that region. Future works will focus on the understanding of such behaviour discovering whether final quality can be linked with those phenomena.

Comparing the three temporal behaviours is observed that the length of the melt pool stabilizes first to its mean value with respect to width and area. This is due to the scan path geometry: at each scanned line the full geometry length is scanned whereas the width is increasing. Accordingly, after few scanned vertical lines the length of the melt pool stabilizes at its mean value without much dependency of the laser movement. Area

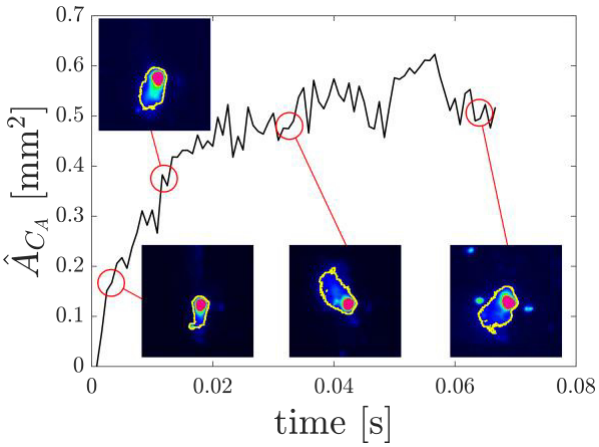

Figure 11: Zoom of the melt pool transient at the beginning of the scan geometry (27th layer).

and width increases until the scanned geometry is large enough and then stabilizes (Fig. 11). Length stabilization takes about 0.02s while area and width stabilization take about 0.05s corresponding to 7 and 17 scanned vertical lines respectively.

C. Real time applications

The average computing time for the HTB algorithm is about 0.5ms per frame. This computing time refers to the compiled version of the code and can further be improved by dedicated hardware setups (e.g. FPGA's [16]). The proposed method can therefore achieve real time performance being the time between two subsequent frames equal to 0.83ms. This fact opens definitely to the concrete possibility of developing feedback control schemes based on geometrical information. Even if the computing time is lower than the sampling period, there are still many questions for the design of a feedback control that must be addressed. At first, the time required for data transfer has to be accounted. Then, control inputs (process parameters that are adjusted during the manufacture) have to be identified and chosen; the choice may also depend on dynamic performance of the SLM system, that have to be *sufficient* for the online adaption of process parameters, i.e. input actuation has to be fast enough to stay within the sampling period. Usual requirements are that control inputs could be controlled one order magnitude faster than the sampling rate, i.e. in the range of 10kHz. Common CNCs and other industrial control units have not such performances, therefore the most promising control input is not scan speed, but laser power controlled via temporal modulation.

As an alternative, to improve process repeatability and in some way control the manufacture, the application of remelting strategies on points detected by in situ real time monitoring should be considered. Assuming that the implemented sample rate is sufficient to detect process stability, the proposed method represents a valuable solution both for accuracy and limited cost of equipment after calibration is performed. In fact, the highest cost of the proposed setup lies in the external lighting system; in an industrial scenario, external lighting system would be used only by the manufacturer and not mounted in all industrial machines.

As a final remark, the class of process dynamics that can be detected is in the range of hundreds of Hz because of the sampling frequency is 1200Hz. This means that some really fast phenomena strictly related to the melt pool (e.g. melt pool oscillations) cannot be observed by such system. On the other hand, the possibility to inspect melt pool shape and spatter ejection is demonstrated. As a result, the method can be used to control dimensions of the melt pool, ensure standard operating conditions and prevent process drifts. In addition, the dependency of melt pool shape with respect to scan path can controlled using a feedback control scheme in place of ad-hoc process parameters allowing for cost reduction. This could be useful especially when "thin-walls-like" geometries (Fig. 2) are produced where overheating effects cause the melt pool being large.

VI. Conclusions

The complementary use of external illumination and process emission for estimation of the melt pool geometry is described. The study presents a new and quantitative calibration method based on externally illuminated images that offers the possibility to estimate melt pool geometry by process emission images. The method proposes an information transfer from externally illuminated to process emission images; the final scheme is based only on process emission images and can be implemented in industrial scenarios due to the relative low cost of the monitoring system.

Process dynamics characterization capabilities are shown: time trends can capture changes in melt pool shape, periodic phenomena, spatter ejection and potentially defects formation. In addition, the presented strategy offers the possibility of real time monitoring in the range of kHz. Due to its computing time performances it can possibly become a source of information for the development of a feedback control or for the implementation of correcting strategies to be applied layer wise (e.g. remelting).

Future work will focus on the following points:

1. the sensitivity of melt pool geometrical estimates with respect to the HTB algorithm would be studied to improve reliability. The

introduction of additional optical elements will be considered to improve image quality;
2. simultaneous acquisition of both externally illuminated images and process emission ones will be implemented to improve calibration;
3. the difference in shape between the results of the HTB algorithm and real melt pool geometry will be investigated;
4. the dependency between scan geometry and melt pool shape will be investigated;
5. the relationship between melt pool shape and quality of produced pieces will be analysed;
6. correcting strategies aiming at keeping the melt pool shape constant will be introduced both in real time and layer wise.

Acknowledgements

The authors would like to acknowledge BLMGroup for the technical support and hardware for external illumination. This work was supported by the Autonomous Province of Trento, through the Regional Law 6/98. Name of the granted Project: LT4.0. Furthermore, this study was supported by the Lombardy Region under the project MADE4LO within the call "POR FESR 2014-2020 ASSE I-AZIONE I.1B.1.3".

References

[1] B. Regaard, S. Kaierle, W. Schulz, and A. Moalem, "Advantages of coaxial illumination for monitoring and control of laser material processing," Proc. ICALEO, vol. 136, pp. 915–919, 2005.

[2] L. Caprio, A. G. Demir, and B. Previtali, "Comparative study between cw and pw emissions in selective laser melting," Proc. ICALEO, p. 1304, 2017.

[3] U. Thombansen and P. Abels, "Process observation in selective laser melting (SLM)," in High-Power Laser Materials Processing: Lasers, Beam Delivery, Diagnostics, and Applications IV, vol. 9356. International Society for Optics and Photonics, 2015, p. 93560R.

[4] T. Craeghs, S. Clijsters, E. Yasa, F. Bechmann, S. Berumen, and J.P. Kruth, "Determination of geometrical factors in layerwise laser melting using optical process monitoring," Optics and Lasers in Engineering, vol. 49, no. 12, pp. 1440–1446, 2011.

[5] F. Dorsch, H. Braun, S. Keßler, D. Pfitzner, and V. Rominger, "Online characterization of laser beam welds by NIR-camera observation," F. Dorsch, Ed., 2013, p. 86030R.

[6] C. H. Kim, D. C. Ahn, "Coaxial monitoring of keyhole during Yb:YAG laser welding", Optics and Laser Technology, vol. 44, pp.1874-1880, 2012.

[7] F. Dorsch, H. Braun, S. Keßler, D. Pfitzner, V. Rominger, "Detection of faults in laser beam welds by near-infrared camera observation," Proc. ICALEO, 2012.

[8] A. G. Demir, L. Monguzzi, and B. Previtali, "Selective laser melting of pure Zn with high density for biodegradable implant manufacturing," Additive Manufacturing, vol. 15, pp. 20–28, 2017.

[9] A. Gökhan Demir, C. De Giorgi, and B. Previtali, "Design and implementation of a multisensor coaxial monitoring system with correction strategies for selective laser melting of a maraging steel," Journal of Manufacturing Science and Engineering, vol. 140, no. 4, pp. 041003–041003–14.

[10] K. Kempen, B. Vrancken, S. Buls, L. Thijs, J. Van Humbeeck, and J. Kruth, "Selective laser melting of crack-free high density m2 high speed steel parts by baseplate preheating," J. Manuf. Sci. Eng., vol. 136, p. 61026, 2014.

[11] T. G. Spears and S. A. Gold, "In-process sensing in selective laser melting (SLM) additive manufacturing," Integr. Mater. Manuf. Innov., 2016.

[12] M. Ester, H.-P. Kriegel, J. Sander, and X. Xu, "A density-based algorithm for discovering clusters in large spatial databases with noise," Proceedings of the 2nd International Conference on Knowledge Discovery and Data Mining (KDD'96), pp. 226–231, 1996.

[13] C. Sammut, G. I. Webb, "Encyclopedia of Machine Learning and Data Mining", pp. 349-353, 2011

[14] A. Dhua, D. N. Sarma, S. Singh, and B. Roy, "Segmentation of images using density-based algorithms," International Journal of Advanced Research in Computer and Communication Engineering, vol. 4, no. 5, pp. 273–277, 2015.

[15] R. D. Kumar, K. Ramareddy, and B. Rao, "A simple region descriptor based on object area per scan line," International Journal of Computer Applications, vol. 3, no. 7, pp. 24–27, 2010.

[16] S. Clijsters, T. Craeghs, S. Buls, K. Kempen, and J.-P. Kruth, "In situ quality control of the selective laser melting process using a high-speed, real-time melt pool monitoring system," Int J Adv Manuf Technol, vol. 75, pp. 1089–1101, 2014.

[17] S. Fujinaga, H. Takenaka, and T. Narikiyo, “Direct observation of keyhole behaviour during pulse modulated high-power nd yag laser,” Appl. Phys. A Mater. Sci. Process., vol. 492.

[18] C. Kägeler and M. Schmidt, “Frequency-based analysis of weld pool dynamics and keyhole oscillations at laser beam welding of galvanized steel sheet,” Phys. Procedia, vol. 5, pp. 447–453, 2010.

[19] T. Furumoto, T. Ueda, M. R. Alkahari, and A. Hosokawa, “Investigation of laser consolidation process for metal powder by two-color pyrometer and high-speed video camera,” CIRP Annals, vol. 62, no. 1, pp. 223–226, 2013.

[20] T. Craeghs, S. Clijsters, J. P. Kruth, F. Bechmann, and M. C. Ebert, “Detection of process failures in layerwise laser melting with optical process monitoring,” Physics Procedia, vol. 39, pp. 753–759, 2012.

Meet the Authors

Matteo Pacher was born in Trento on the 8th of March 1991. He received the M.S. degree in Mechatronics Engineering at the University of Trento, Italy, in 2016. Currently he is a PhD candidate at the Mechanical Department of the Politecnico di Milano. His research interests include: process monitoring, system identification and control, laser cutting and process automation.

Luca Mazzoleni was born in Bergamo on the 19th of March 1993. Currently he is a M.S. student in Mechanical Engineering at the Politecnico di Milano. His research interests and his Master Thesis include: Selective Laser Melting, Coaxial process monitoring by means of fast cameras and different external illumination sources, laser material interaction and process automation.

Leonardo Caprio was born in 1993 and graduated in Mechanical Engineering with specialisation in Advanced Materials and Manufacturing from the Politecnico di Milano in 2017. Currently he is a PhD candidate at the Mechanical Department of the Politecnico di Milano. His research is currently focused on the Selective Laser Melting technology in the field of Additive Manufacturing at the AddMe.Lab of the Politecnico di Milano.

Ali G¨okhan Demir was born in Istanbul, Turkey, in 1985. He received the M.Sc. degree in mechanical engineering and European Ph.D. degree in mechanical engineering from the Politecnico di Milano, Italy, in 2009 and 2014, respectively. He has been Assistant Professor with the department of Mechanical Engineering, Politecnico di Milano, since 2015. He has authored over 50 papers in international journals and international conference proceedings. His current research interests include laser-based manufacturing processes, mainly, additive manufacturing, laser micromachining, and process monitoring with the SITEC - Laboratory for Laser Applications.

Barbara Previtali received the Ph.D. degree in manufacturing and production system from the Politecnico di Milano, Milan, Italy, in 2002. In 2016, she was appointed as Full Professor in the Mechanical Engineering Department, Politecnico di Milano. She leads the SITEC—Laboratory for Laser Applications and PromozioneL@ser with AITeM, which collects Italian laser users in industry and academia. Her current research interests include modeling, optimization and control of laser processes in their application in various fields. On these research subjects, she has authored or coauthored over 100 papers in refereed international journals and international conferences and two international patents.